Tensor network simulation for the frustrated J_1-J_2 Ising model on the square lattice

Hong Li[1,*] and Li-Ping Yang[2,†]

[1]Department of Physics, Renmin University of China, Beijing 100872, China
[2]Department of Physics, Chongqing University, Chongqing 401331, China

By the extensive tensor network algorithms, we provide the phase diagram of the frustrated J_1-J_2 Ising model on the square lattice. Based on the fine numerical simulations, we discuss the cases with controversy in the phase diagram, especially for the stripe transition in the regime $g = |J_2/J_1| > 1/2$, $(J_2 > 0, J_1 < 0)$. Our simulations suggest that the first-order phase transition may reside in a very narrow parameter region $1/2 < g < g^*$ (g^* is much smaller than previous research). Combining with the analysis of critical properties, we find the evidence that the classical J_1-J_2 model evolves continously from two decoupled Ising models ($g \to \infty$ with central charge $c = 1$) to a point of tricritical Ising model (with $c = 0.7$) as g decreases to g^*.

I. INTRODUCTION

In 1944, Onsager provided the rigorous solution of the two-dimensional classical Ising model[1], which greatly deepened and enriched the understanding of the phase transition. As a generalization of this model, the next-nearest neighbor interaction J_2 is introduced, however, the overall phase diagram and phase transition are still under debate. There is a rough physical picture as follows: for the frustrated J_1-J_2 Ising model, in the low temperature case, the system lies in the ferromagnetic (FM) order phase when $g = J_2/|J_1| < 1/2$, corresponding to Z_2 symmetry breaking; while $g > 1/2$, the system enters the stripe antiferromagnetic (SAFM) phase, also called collinear antiferromagnetic phase with Z_4 symmetry breaking.

Compared to the corresponding quantum model, both the theoretical explanation and numerical simulations are easier in the classical case, which can unveil some common properties of the frustrated systems. In particular, the SAFM phase is of great interest because a moderate external field can induce the nematic phase adjacent to it[2, 3]. It is believed that the nematic phase will be useful to understand the high temperature superconductor[4–6].

The early research shows that, the phase transition between two ordered phases and paramagnetic phase is of continuous type. It is accepted that the phase transition is of Ising universal class in the case of $g < 1/2$, while holds weak universality[7–13] in the case of $g > 1/2$. For example, some critical exponents depend on the details of the interactions and therefore vary with coupling parameters[14]. In conformal field theory (CFT), a phase transition with varying critical exponents is possible for central charge $c \geq 1$. Since 1990s, a lot of calculations, mostly based on cluster-variation method (CVM) and Monte Carlo (MC) simulations, show that $1/2 < g < g^*$, $(g^* \simeq 1)$, the phase transition is of the first order[15–21], while other simulations for some given $g < g^*$ prefer the conclusion of weakly universal continuous phase transition[22–25].

The upper limit g^* keeps decreasing with the numerical simulations improving. In the range $1/2 < g \leq 0.9$, the phase transition between striped phase and paramagnetic phase was determined as the weak first order by MC simulation[26]. However, the smaller g above $1/2$, the bigger the system size is needed for the reliable MC simulation. Whereafter, Jin *et al.* concluded that $g^* \simeq 0.67$ by numerically mapping J_1-J_2 model to Ashkin-Teller (AT) model also with Z_4 symmetry breaking[27, 28]. In addition, they claimed the pseudo-first-order behavior at $g \gtrsim g^*$. MC simulations with larger system size strengthened their conclusion[29] and recent cluster mean-field (CMF)[30] also mentioned the consistent results.

Reaching the conclusion of both weak first-order phase transition and continuous phase transition with pseudo-first-order behaviors, the finite-size effect is a challenge what MC and CVM simulations face. The tensor network algorithms we adopt can approach the thermodynamic limit. Recently, it was applied to calculate J_1-J_2 frustrated model[31], and fix the Berezinskii-Kosterlitz-Thouless phase transition in the classical clock model[32]. The tensor renormalization group performed well in the spin glass model[33]. Based on higher-order singular value decomposition (abbreviated as HOTRG) simulation for three dimensional Ising model fixed the phase transition temperature to the seventh decimal place[34]. The projected entangled simplex state scenario brought the remarkable breakthrough in the quantum frustration model[35, 36].

In this article, combining infinite time-evolving block decimation (iTEBD)[37, 38] and HOTRG, we try to provide the full phase diagram and discuss the nature of the phase transition. We find that the line of first-order phase transition may not exist or lie in a much smaller region than previous research when $g > 1/2$. As g goes down to about $1/2$, the central charge of the model decreases from 1 (two decoupled Ising model) to about 0.7, which corresponds to tricritical Ising (TCI) model. This result is also strengthened by the calculation from matrix-product operator (MPO) scenario based on the Klein bottle (KB) entropy method[39].

*157luoluoluo@ruc.edu.cn
†liping2012@cqu.edu.cn

The article is arranged as follows: In Sec. II, we will introduce the model and the related formulation based on iTEBD and HOTRG. We employ iTEBD to simulate the physical quantities. HOTRG helps us to extract the critical information from the fixed point tensor during the renormalization group (RG) flow, except which there is another way to fit the central charge by the calculation combining MPO and Klein bottle entropy[39]. In Sec. III, we demonstrate and disscuss our numerical results: the phase diagram and the critical properties. Finally, we go to the conclusion in Sec. IV.

II. MODEL AND METHODS

The Hamiltonian of J_1-J_2 model is written as

$$H = J_1 \sum_{\langle ij \rangle} \sigma_i \sigma_j + J_2 \sum_{\langle\langle ij \rangle\rangle} \sigma_i \sigma_j. \tag{1}$$

Here, $\sigma = \pm 1$, and J_1, J_2 mean the coupling parameters, corresponding to ferromagnetic ($J_1 < 0$) nearest neighbour pair denoted by $\langle ij \rangle$ and antiferromagnetic ($J_2 > 0$) next-nearest neighbour pair denoted by $\langle\langle ij \rangle\rangle$ respectively. For convenience, we set $J_1 = -1, J_2 = g$ hereafter.

A. The calculation of the physical quantities

On the square lattice, the partition function of this model is expressed to sum over the Boltzmann factor related to the configuration $\{\sigma\}$

$$Z = \sum_{\{\sigma\}} e^{-\beta H\{\sigma\}} = \mathrm{Tr}(TSTS...). \tag{2}$$

There are two types of tensors as shown in Fig. 1(a): one is T defined on the center of the square unit, and the other is S defined on the lattice site. T and S both hold the reflection symmetry along $x-$ and $y-$ directions, with the following expressions:

$$\begin{aligned} T_{lrud} &= e^{\frac{\beta}{2}(\sigma_l\sigma_u+\sigma_u\sigma_r+\sigma_r\sigma_d+\sigma_d\sigma_l)-\beta g(\sigma_l\sigma_r+\sigma_u\sigma_d)}, \\ S_{lrud} &= \delta_{lrud} = \begin{cases} 1, & l=r=u=d \\ 0, & \text{others} \end{cases}, \end{aligned} \tag{3}$$

where $\sigma_{l,r,u,d}$ refers to the four spin variables (left, right, up, down) as the tensor indices emiting from T. As a consequence, we obtain a tensor network with 2×2 structure as the unit cell, then by coarse-graining, T_0 is formulated as the single site tensor shown in Fig. 1(b). Comparing to the original lattice, the tensor network formed by T_0 carries a rotation angle $\pi/4$.

For the calculation of any physical quantity O, the one that only one site tensor T is encoded by O (labelled as T^O) with the other tensors invariant, is called the "impurity" site method. In this scheme, the internal energy

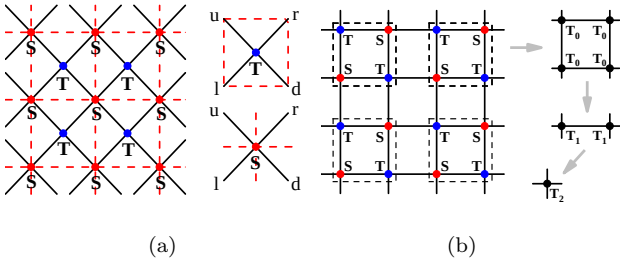

FIG. 1: (a) Defintion of tensor with four indices l, r, u, d. (b) Demonstration of coarse graining, by which T_0 forms the single site unit from the original unit cell 2×2 (enclosed by the dash line).

U, the magnetization m, and the stripe magnetization $m_s = \sqrt{m_x^2 + m_y^2}$ are defined as follows:

$$\begin{aligned} T^U_{lrud} &= -\frac{1}{2}[(\sigma_l\sigma_u + \sigma_u\sigma_r + \sigma_r\sigma_d + \sigma_d\sigma_l) \\ &\quad + g(\sigma_l\sigma_r + \sigma_u\sigma_d)] \times T_{lrud}, \\ T^m_{lrud} &= \frac{1}{4}(\sigma_l + \sigma_r + \sigma_u + \sigma_d) \times T_{lrud}, \\ T^{m_y}_{lrud} &= \frac{1}{4}(\sigma_l - \sigma_r - \sigma_u + \sigma_d) \times T_{lrud}, \\ T^{m_x}_{lrud} &= \frac{1}{4}(\sigma_l - \sigma_r + \sigma_u - \sigma_d) \times T_{lrud}. \end{aligned} \tag{4}$$

The key point of iTEBD lies on the row-by-row projection based on the power method. Finally the converged matrix product state (MPS) is obtained. The alternative way to locate the phase transition point is by the singularity of the converged MPS. By the normalized entanglement spectrum $\{\lambda_1, \lambda_2, ..., \lambda_j, ...\}$, with $\sum_j \lambda_j^2 = 1$, the entanglement entropy reads as follows:

$$S_E = -\sum_j \lambda_j^2 \ln(\lambda_j^2). \tag{5}$$

Meanwhile, the correlation length can be calculated by the largest and the second largest eigenvalues ϵ_1, ϵ_2 of the reduced matrix corresponding to the MPS:

$$\xi = -\frac{1}{\ln|\epsilon_2/\epsilon_1|}. \tag{6}$$

B. The extraction of the critical properties

In the framework of the HOTRG[34], coarse-graining is the RG process, during which CFT information is encoded in the fixed-point tensor $T^*(= T^{(i)}/\sum_{lu} T^{(i)}_{lluu})$, where $T^{(i)}$ is the tensor unit in the i-th RG process and T^* keeps invariant[40].

Then, we get $M_{u,d} = \sum_l T^*_{llud}$, with eigenvalues: $\lambda_0, \lambda_1, ..., \lambda_m, ...$(descending order), by which the central

charge c and scaling dimension h_m read as[40]:

$$\begin{aligned} c &= \frac{6}{\pi}\ln\lambda_0, \\ h_m &= -\frac{1}{2\pi}\ln(\lambda_m/\lambda_0). \end{aligned} \tag{7}$$

There is another way to obtain c by fitting based on Eq. (8). The partition functions with the torus and Klein bottle boundary conditions are written respectively as[39]:

$$\begin{aligned} \ln Z^T &\simeq -f_0 L_x L_y + \frac{\pi c}{6L_y} L_x, \\ \ln Z^K &\simeq -f_0 L_x L_y + \frac{\pi c}{24L_y} L_x + S_{\mathrm{KB}}. \end{aligned} \tag{8}$$

Here, S_{KB} refers to Klein bottle entropy[41] relevant to the boundary, which is universal. Given $L_x \gg L_y$, the calculation is validated by Eq. (8). We adopt iTEBD scheme to treat MPO, and use the canonicalization for truncation. Finally, we can calculate S_{KB} and the central charge c.

III. NUMERICAL RESULTS

A. Phase diagram and physical quantities

By iTEBD, combing the entanglement entropy with the magnetization, the phase diagram is determined as shown in Fig. 2. It is worthwhile to note that the point located exactly $g = 0.5$ is not from our calculation. $g = 0.5$ renders the high degeneracy of the ground state, which invalidates the power method scenario. Thus we choose HOTRG for the calculation. However, the physical quantities can not go to the convegence with the kept bond dimension D increasing. There exist a few research about $g = 0.5$ supporting finite phase transition temperature[42–44], but the most claim that the critical temperature is suppressed to zero temperature due to the high degeneracy, just like one-dimensional system[9, 11, 15, 20, 21, 24]. We put $g = 0.5, T_c = 0$ in the phase diagram.

There are three phases in Fig. 2. In the neighbourhood of $g = 0.5$, the numerical results converge well. The detailed simulations are done at two points $g = 0.46$, 0.55 besides $g = 0.5$. $g = 0.55$ is claimed to be in the region of weak first-order phase transition as mentioned above. As for $g = 0.46$, it is widely accepted that the phase transition in the whole parameter region of $g < 1/2$ is continuous and belongs to the Ising universal class before 2013[16, 21, 24, 25, 45]. However, the analyses with CMF[28] and effective-field theory[46] suggest that the model may also has a transition line of first order close to $g = 1/2$ when $g < 1/2$.

As is shown in Fig. 3, we compare the results with the different truncation dimension D with 10^{-3} temperature interval. It seems that there is a jump in the temperature

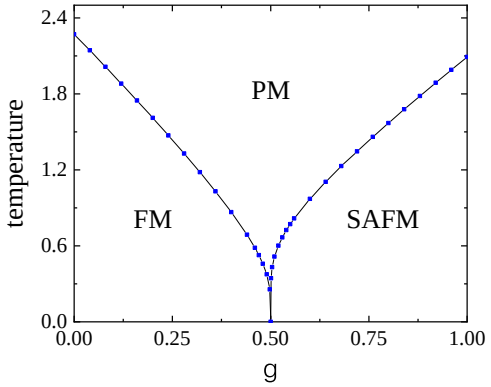

FIG. 2: The phase diagram in the parameter space: the temperature and the relative coupling g. There are three separated phases: ferromagnetic phase (FM), stripe antiferromagnetic phase (SAFM), and paramagnetic phase (PM) with blue phase boundary lines.

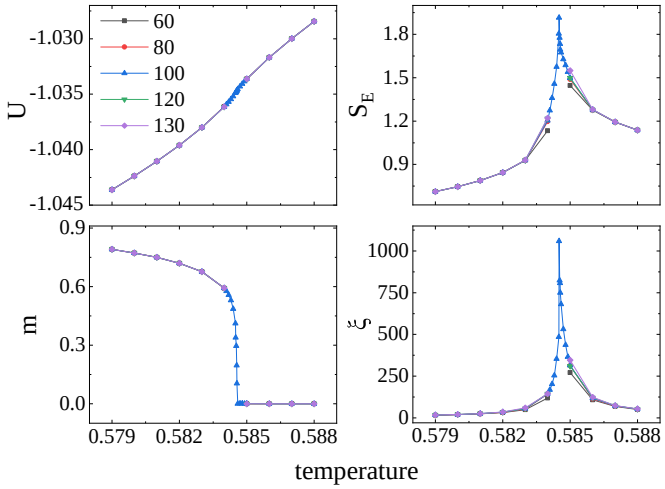

FIG. 3: The physical quantities: the internal energy (U), magnetization (m), entanglement entropy (S_E), and correlation length (ξ) as a function of the temperature at $g = 0.46$. The selected bond dimension D is $60, 80, 100, 120, 130$ respectively by iTEBD in the framework of "impurity" method.

range $(0.584, 0.585)$, in which we add the fine data with 10^{-5} temperature interval with fixed $D = 100$. Then the "jump" becomes smaller in the magetization, and there is not discontinuity in the internal energy. As a consequence, the phase transition at $g = 0.46$ is of continuous type, and belongs to the Ising universal class which we can prove below. The recent work using CMF provides the same conclusion[30].

Now we move to the case of $g = 0.55$. The similar calculation is done, as is shown in Fig. 4. The order parameter is the stripe magnetization m_s with Z_4 symmetry breaking. The refined data (the smallest temperature interval is 10^{-6}) is from $D = 120$. The convergence error

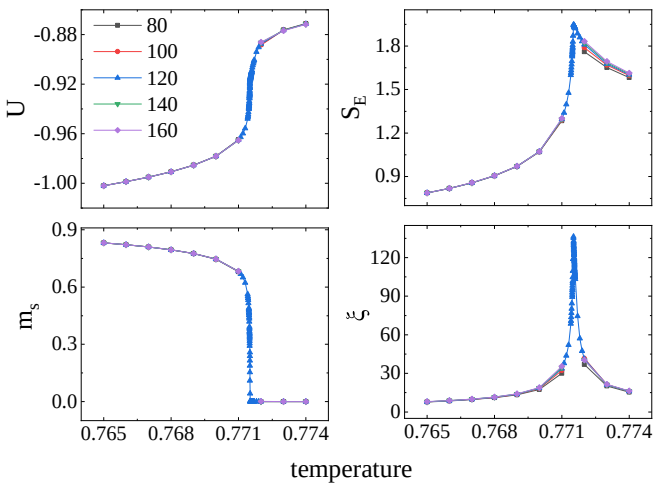

FIG. 4: The physical quantities: the internal energy (U), stripe magnetization (m_s), entanglement entropy (S_E) and correlation length (ξ) as a function of the temperature at $g = 0.55$. D is taken as $80, 100, 120, 140, 160$ respectively by iTEBD in the framework of "impurity" method.

of MPS entanglement spectrum reaches 10^{-13} at almost all selected temperature points, and converges to 10^{-8} at only three temperature points, which are extremely close to the phase transition. The curves of internal energy U and magnetization m_s are very steep around the critical temperature, which become more prominent by contrast with Fig. 3, but the discontinuity gradually disappears when the temperature points are taken more closely. The singularity of the entanglement entropy and correlation length determines the consistent phase transition temperature. The similar discussion holds at $g = 0.55$. The numerical results suggest that it is also continuous phase transition. The phase transition temperature can be read from the location of the sharp peak in the entanglement entropy and correlation length.

In particular, we test $D = 160$ for the convergence check in the case of $g = 0.55$, which is harder to simulate with high precision. To discern the phase transition type, especially in between the weak first-order and the continuous, it demands high numerical simulation precision. The conclusion that the weak first-order phase transition in the narrow region $1/2 < g < g^*$ may be just a consequence of undistinguishable continuous change signal in physical quantities near phase transition.

B. The criticality and universality

In the scheme of HOTRG, the critical information is extracted from the fixed point tensor in the RG flow. The central charge c and the scaling dimension h_1 can be obtained by Eq. (7). During the tensor contraction, the size of the system reduces to one half after one coarse-graining, i.e. the decay of the system size is in exponential way. After n-th RG procedure, the system size calculated reaches $L = 2^n$. Correspondingly, the perturbation introduced by the truncation error will gradually destroy the fixed-point tensor with n increasing. As a result, c, h_1 diverge quickly, as shown in Fig. 5. We can observe that the central charge c decreases from about 1 (the decoupled Ising limit) to 0.7 and h_1 changes to 0.075 (TCI universality), as g approaches g^* before complete instability.

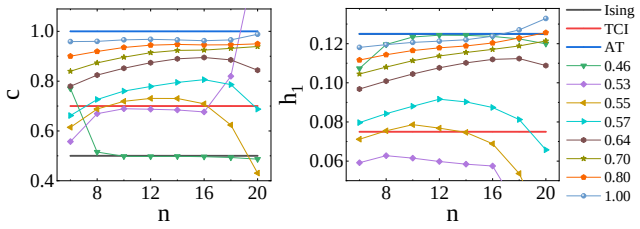

FIG. 5: c, h_1 vary with n (RG step) from HOTRG with $D = 100$. For reference, three types of universal class are shown: Ising ($c = 0.5$, $h_1 = 0.125$), TCI ($c = 0.7$, $h_1 = 0.075$), and AT ($c = 1$,$h_1 = 0.125$).

The TCI Hamiltonian[47] can be written as

$$H = -\sum_{\langle ij \rangle}(K + \delta_{\sigma_i\sigma_j}) - \mu \sum_i \sigma_i^2. \tag{9}$$

Here, σ_i^2 equals 0 when the site is vacant otherwise 1. K is the energy of a pair of unlike spins, and $K+1$ that of a pair of like spins. The chemical potential μ specifies the average occupation number on the lattice. Due to one more option of vacancy, there is the coexistence of the three phases, where $c = 0.7$[47].

It can be observed that as g deviates from 1, the curves of c and h_1 varying with RG step become more and more uneven, and the closer g gets to $1/2$, the faster they diverge. This agrees with our argument above, that the phase transition is accompanied by a significant change in U and m_s when g is close to $1/2$, thus it is rather difficult to fix the phase boundary and the fixed-point tensor in the RG flow.

Besides the RG scenario, we also choose a moderate way to contract the tensor network for the crosscheck. MPO in one row is treated as the transfer matrix, then the system shrinks row by row rather than in exponential way. The alternative way to extract the critical properties is from CFT formula in Eq. (8). We set $L_x \to \infty$, finite L_y guarantees the requirement $L_x \gg L_y$ in Eq. (8). The linearity in the fitting of $\ln Z/(L_x L_y)$ versus $\pi/(6{L_y}^2)$ keeps very well in the list of Table. I, which also indicates the feature of the continuous phase transition.

The fitting result of central charge decreases with decreasing g ($> 1/2$), consistent with the result of HOTRG as demonstrated above. The monotonic behaviors also conform to the c theorem of 2D renormalizable field theory[48]. However, the calculation[26] in the scenario of

transfer matrix doesn't conform to the c theorem, where c increases with g decreasing.

In terms of the consistence with the c theorem in our simulations, there are two points needed to be addressed. On the one hand, starting from decoupled Ising limit, the lattice should be considered in the direction of $\pi/4$, then treats J_1 as perturbation. We thus use T_0 in Fig. 1 as initial tensor. On the other hand, the application of small L_y does not suffice to the critical property although there is not truncation error in the numerical simulation. With regard to this point, we adopt iTEBD scheme to treat MPO and use the canonicalization for truncation to reach large L_y in our work.

g	c	g	c	g	c
0.46	0.499	0.57	0.736	0.70	0.925
0.53	0.631	0.58	0.760	0.80	0.933
0.55	0.690	0.60	0.802	1.00	0.978
0.56	0.708	0.64	0.864	2.00	1.004

TABLE I: Central charge is obtained by fitting $\ln Z/(L_x L_y) \sim \pi/(6{L_y}^2)$ for selected L_y. The results are given by using initial tensor T_0 in Fig. 1.

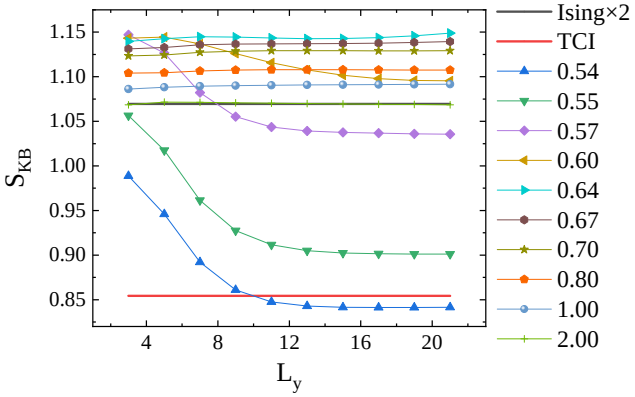

FIG. 6: The Klein bottle entropy is obtained by fitting for different L_y when g takes values in the region $0.5 < g \leq 2$.

Then, we calculate Klein bottle entropy by fitting with $L_x = 100 \sim 200$, using Eq. (8). In Fig. 6, there are two reference lines[41, 47]:

$$S_{\rm KB} = 2 \times \ln(1+\sqrt{2}/2) \approx 1.0696, \quad \text{(Ising} \times 2\text{)}$$

$$S_{\rm KB} = \ln\left[\frac{(2+\sqrt{2})(s_1+s_2)}{2\sqrt{s_1^2+s_2^2}}\right] \approx 0.8543. \quad \text{(TCI)}$$

Here, $s_1 = \sin(2\pi/5), s_2 = \sin(4\pi/5)$. In the case of $g = 2$, the calculated $S_{\rm KB}$ matches the theoretical value of the two decoupled Ising models. In the regime $0.5 < g < 2$, the curves of $S_{\rm KB}$ separated into two bundles. As g decreases from 2, the curves gradually deviate from the two-Ising line but still remain very even. When $g < 0.64$, a drop in $S_{\rm KB}$ starts to be developed for small L_y, then the curve stabilizes at a value for larger L_y. Whereafter, the $S_{\rm KB}$ decreases as g decreases to about $1/2$, and reaches about the value of TCI model at $g^* \approx 0.54$. The combination of HOTRG and KB entropy suggest the following picture: J_1-J_2 model evolves continuously from two decoupled Ising models (with $c = 1, h_1 = 0.125$) to a point of tricritical Ising (TCI) model (with $c = 0.7, h_1 = 0.075$) as g decreases to g^*.

IV. CONCLUSIONS

In summary, we exploit the extensive tensor-network algorithms, to determine the phase diagram and analyze the critical properties of the classical J_1-J_2 model. For the cases under debate, we perform detailed simulations. Our numerical results clearly show that the phase transition between FM and PM phase is of Ising universal class when $g < 1/2$. For the phase transition between striped and paramagnetic phase, the results from MC simulations[27–29] and CVM[30] state that the phase transition is of continuous type only when $g \gtrsim g^*$, $g^* \simeq 0.67$. Our calculation shows that if there is a upper limit g^* for the first-order phase transition, it would be $g^* \simeq 0.54$, corresponding to universal class of TCI type.

The TCI model usually describes the critical region around the tricritical point, at which the continuous Ising phase transition ends or one certain first-order phase transition starts. To this point, it is acceptable that the phase transition is of the first order in the parameter region $0.5 < g \lesssim 0.54$. Although the tensor network algorithms can touch the thermodynamic limit, higher precision is limited to the short-range entanglement near or at criticality in the perspective of the tensor RG flow[49]. In the regime close to $g = 1/2$ demonstrating the universality, there exist the sharp variations in physical quantities, which brings the great challenge for the numerical simulations. It is possible that many previous work to identify the phase transition as a first-order type in the range of $g < g^*$ with a relatively large g^* is limited by the finite-size effect and simulation precision.

However, there is another possibility that for all the cases of $g > 1/2$, the phase transitions are all continuous. the TCI point refers to $g = 0.5 + \delta$ (where δ is a positive infinitesimal), the model evolved continuously from this point to the two decoupled Ising models with $c = 1$. Subjected to the kept dimension D and subsequent lack of precision, our simulations become unstable[50] in the very close neighbourhood of $g = 0.5$, giving rise to the absence of the convincing conclusion. The exploration for the stability and convergence with larger D is ongoing.

V. ACKNOWLEDGEMENT

We are indebted to Zhi-Yuan Xie, Hong-Hao Tu for the inspiring discussions. We thank Adil A. Gangat for the careful reading of the manuscript. This

work was supported by National Science Fundation of China, NSFC(Grant No.11874095, and No.12047564), National Science Fundation of Chongqing(Grant No.cstc2018jcyjAX0399), and Research Funds for the Central Universities (No.2018CDXYWU0025).

[1] L. Onsager, Phys. Rev. **65**, 117 (1944).
[2] A. I. Guerrero, D. A. Stariolo, and N. G. Almarza, Phys. Rev. E **91**, 052123 (2015).
[3] A. I. Guerrero and D. A. Stariolo, Phys. A: Stat. Mech. Appl. **466**, 596 (2017).
[4] P. Chandra, P. Coleman, and A. I. Larkin, Phys. Rev. Lett. **64**, 88 (1990).
[5] C. Fang, H. Yao, W.-F. Tsai, J. P. Hu, and S. A. Kivelson, Phys. Rev. B **77**, 224509 (2008).
[6] R. M. Fernandes, A. V. Chubukov, J. Knolle, I. Eremin, and J. Schmalian, Phys. Rev. B **85**, 024534 (2012).
[7] M. P. Nightingale, Phys. Lett. A **59**, 486 (1977).
[8] R. H. Swendsen and S. Krinsky, Phys. Rev. Lett. **43**, 177 (1979).
[9] J. Oitmaa, J. Phys. A **14**, 1159 (1981).
[10] K. Binder and D. P. Landau, Phys. Rev. B **21**, 1941 (1980).
[11] D. P. Landau, Phys. Rev. B **21**, 1285 (1980).
[12] D. P. Landau and K. Binder, Phys. Rev. B **31**, 5946 (1985).
[13] J. Oitmaa and M. J. Velgakis, J. Phys. A: Math. Gen. **20**, 1269 (1987).
[14] M. Suzuki, Prog. Theor. Phys. **51**, 1992 (1974).
[15] J. L. Morán-López, F. Aguilera-Granja, and J. M. Sanchez, Phys. Rev. B **48**, 3519 (1993).
[16] F. Aguilera-Granja, J. L. Morán-López, J. Phys.: Condens. Matter **5** A195 (1993).
[17] J. L. Morán-López, F. Aguilera-Granja, and J. M. Sanchez, J. Phys.: Condens. Matter **6** 9759 (1994).
[18] E. López-Sandoval, J. L. Morán-López, F. Aguilera-Granja, and J. M. Sanchez, Solid State Commun. **112**, 437 (1999).
[19] R. A. dos Anjos, J. R. Viana, and J. R. de Sousa, Phys. Lett. A **372**, 1180 (2008).
[20] A. Kalz, A. Honecker, S. Fuchs, and T. Pruschke, Eur. Phys. J. B **65**, 533 (2008).
[21] A. Kalz, A. Honecker, S. Fuchs, and T. Pruschke, J. Phys.: Conf. Ser. **145**, 012051 (2009).
[22] N. Jr. Alves and J. R. Drugowich de Felicio, Mod. Phys. Lett. B **17** 209 (2003).
[23] A. Malakisa, P. Kalozoumis, and N. Tyraskis, Eur. Phys. J. B **50**, 63 (2006).
[24] S.-Y. Kim, Phys. Rev. E. **81**. 031120 (2010).
[25] J. H. Lee, H. S. Song, J. M. Kim, and S.-Y. Kim, J. Stat. Mech. P03020 (2010).
[26] A. Kalz, A. Honecker, and M. Moliner, Phys. Rev. B **84**, 174407 (2011).
[27] S. Jin, A. Sen, and A. W. Sandvik, Phys. Rev. Lett. **108**, 045702 (2012).
[28] S. Jin, A. Sen, W. Guo, and A. W. Sandvik, Phys. Rev. B **87**, 144406 (2013).
[29] A. Kalz and A. Honecker, Phys. Rev. B **86**, 134410 (2012).
[30] N. Kellermann, M. Schmidt, and F. M. Zimmer, Phys. Rev. E **99**. 012134 (2019).
[31] A. A. Gangat, and Y.-J. Kao, Phys. Rev. B **100**, 094430 (2019).
[32] Z.-Q. Li, L.-P. Yang, Z. Y. Xie, H.-H. Tu, H.-J. Liao, and T. Xiang, Phys. Rev. E **101**, 060105(R) (2020).
[33] C. Wang, S.-M. Q, and H.-J. Zhou, Phys. Rev. B. **90**, 174201(2014)
[34] Z. Y. Xie, J. Chen, M. P. Qin, J. W. Zhu, L. P. Yang, and T. Xiang, Phys. Rev. B **86**, 045139 (2012).
[35] Z. Y. Xie, J. Chen, J. F. Yu, X. Kong, B. Normand, and T. Xiang, *Phys. Rev. X* **4**, 011025(2014).
[36] H. J. Liao, Z. Y. Xie, J. Chen, Z. Y. Liu, H. D. Xie, R. Z. Huang, B. Normand, and T. Xiang, *Phys. Rev. Lett.* **118**, 137202(2017)
[37] G. Vidal, Phys. Rev. Lett. **98**, 070201 (2007).
[38] R. Orus and G. Vidal, Phys. Rev. B **78**, 155117 (2008).
[39] H.-H. Tu, Phys. Rev. Lett. **119**, 261603 (2017).
[40] Z.-C. Gu and X.-G. Wen, Phys. Rev. B **80**, 155131 (2009).
[41] L. Chen, H.-X. Wang, L. Wang, and W. Li, Phys. Rev. B **96**. 174429 (2017).
[42] Y. Boughaleb, M. Noureddine, and R. Nassif, Physics Research International **2010** 1 (2010).
[43] M.K. Ramazanov, A.K. Murtazaev, and M.A. Magomedov, Solid State Commun. **233**, 35 (2016).
[44] R. Timmons, K. De'Bell, Can. J. Phys. **96**, 912 (2018).
[45] M. D. Grynberg and B. Tanatar, Phys. Rev. B **45**, 2876 (1992).
[46] A. Bobák, T. Lučivjanský, M. Borovský, and M. Žukovič, Phys. Rev. E **91**, 032145 (2015).
[47] P. Di Francesco, P. Mathieu, and D. Senechal, *Conformal Field Theory* (Springer, New York, 1997).
[48] A. B. Zamolodchikov, JETP Lett. **43**, 731 (1986).
[49] G. Evenbly, and G. vidal, Phys. Rev. Lett. **115**, 180405 (2015) ; S. Yang, Z.-C. Gu, and X.-G. Wen, Phys. Rev. Lett. **118**, 110504 (2017).
[50] D. Kadoh, Y. Kuramashi, and R. Ueno, Prog. Theor. Exp. Phys. 061B01 (2019)